

MECHANISMS OF IMPURITY EFFECT AND DUCTILITY ENHANCEMENT OF MO AND CR ALLOYS

N. Ma¹, B.R. Cooper¹, C.-Y. Feng², and B. S.-J. Kang²

¹Physics Department

²Mechanical and Aerospace Engineering Department

West Virginia University

Morgantown, WV 26506

ABSTRACT

The objective of this research is to understand and minimize the impurity effect for room-temperature ductility improvement of Mo- and Cr-based alloys by the inclusion of suitable metal oxide dispersions. Mo- and Cr-based alloys are brittle at room temperature due to oxygen and nitrogen embrittlement, respectively. Past research showed that suitable amount of MgO or MgAl₂O₄ dispersion can improve the room temperature tensile ductility of Cr or Mo alloys. However, the experimental results showed inconsistent room-temperature ductility behavior with alloys under similar composition and processing conditions. The purpose of this research is (i) to identify the mechanisms responsible for the impurity embrittling and to tailor ductility enhancement based on fundamental atomistic electronic structure analysis, which will guide the selection of suitable nano-sized metal oxides to be incorporated in the Mo or Cr alloys to achieve the desirable room-temperature ductility, and (ii) to further develop a micro-indentation technique suitable for in-situ mechanical property measurement and ductile/brittle evaluation.

On the first research task, using *ab-initio* FP-LMTO techniques, we investigate the electronic structures of Mo and Cr, with possible embrittling impurities (nitrogen or oxygen) and with or without MgO layers. The corresponding electronic structures and chemical bonds near the surface boundaries are calculated. Based on these results and by extending the Rice's criterion, we propose several hypotheses to explain the mechanism of impurity effect and ductility enhancement of Mo and Cr alloys. In addition, we developed *ab-initio* database for more efficient tight-binding schemes. Such schemes are suitable to study some of the dynamic effects, such as impurity gettering and defects transport, that are pertinent to the ductility enhancement mechanism. We also conduct large scale simulations (10^4 - 10^5 atoms) for the purpose of understanding the qualitative effect of varying the dispersion particle sizes.

On the second research task, we have further developed and refined a micro-indentation technique suitable for in-situ material mechanical properties and ductility/brittle evaluation of small-size sample alloys. Theoretical background, experimental verification, and some preliminary test results are presented.

INTRODUCTION

Due to their ultra-high working temperature (>1000°C) and excellent oxidation and corrosion resistance, a number of Cr and Mo based alloys are being developed as the next generation structural

materials for fossil energy applications. However, a severe drawback with these material systems is the limited room-temperature ductility. It has been known that certain species of trace elements, including nitrogen (N) and oxygen (O), can cause embrittlement of Cr and Mo alloys, respectively. For example, the ductile-to-brittle transition temperature (DBTT) of pure Cr (with less than 0.0001 atomic pct of N) is within the ambient temperature range, while that of unalloyed recrystallized Cr with commercial purity is approximately 150°C in tension [1]. There have been numerous studies concerning improving the ductility of Cr- and Mo-based alloys at ambient temperature. In order to stabilize or remove the interstitial impurities, scavenging elements, such as tungsten, molybdenum, and rhenium were alloyed with Cr resulting in increased ductility [2]. Another route was demonstrated by Brady *et.al.* [3] that suitable amount of MgO dispersion improves the room temperature tensile ductility of Cr by 10-20%. Based on microstructural analysis with TEM imaging techniques, they found the oxide dispersions attracted the detrimental agents (notably N and S) to precipitate near the oxide-metal interface. Therefore, detrimental impurity management mechanism (i.e., by preventing the detrimental impurities from segregating to the Cr grain boundaries) has been invoked to explain the ductility enhancement. Interestingly, similar microstructures were discovered in their later experiments using La₂O₃, TiO₂ and Y₂O₃ as dispersions, but none displayed any ductility enhancement. This indicates that other factors, perhaps hiding at deeper levels below the microstructures, are contributing to the Cr's ductility enhancement.

This research contains two research tasks: (i) to conduct atomistic computational modeling and simulations on the study of impurity embrittlement and metal oxides ductility enhancement mechanism in Mo and Cr alloys, and (ii) to continue the development of a micro-indentation technique suitable for in-situ material mechanical property measurement and ductile/brittle characterization of the various small-size Mo and Cr alloys studied in this research project.

TASK 1: ATOMISTIC MODELING AND SIMULATION

The classic theory of Griffith [1, 4] demonstrates that brittle fracture will occur when the hosting material can stably sustain an atomically sharp crack in the lattice without breakdown by dislocation generation. Therefore, the characteristic failure mode of a material depends on the relative easiness of creating new surfaces compared with forming and emitting dislocations. Based on this theory, Rice [5] proposed a criterion to quantitatively measure the tendency of a material to be brittle or ductile in terms of the ratio of the energies for surface and dislocation formation. In practice, however, this criterion has limited applications because a system's total energies can be affected by many other non-relevant factors, which makes it difficult to obtain the relevant energetics for the ideal cleavage and stacking fault configurations, due to the lack of *ab-initio* knowledge of the rich variety of interactions among the imperfections within the system, including impurities, dislocations, cracks, and grain boundaries at quite different length scales. At the basic fundamental level, the mechanisms responsible for the impurity and additive effects are still largely unknown.

In this work, we attempt to extend the Rice's criterion and proposed several hypotheses that enable us to conveniently study the impurity effect on material ductility. These new hypotheses are based on the

properties of the valence electrons that participate in forming chemical bonds between atoms in solids. The knowledge of the valence electrons will then translate into that of the chemical bonds, and hence their ductile or brittle mechanical properties through Rice's criterion. Comparing to the energetics approach, the one based on electronic structure analysis will provide a more comprehensive understanding of the mechanisms from a deeper level, yet it involves standard techniques that are readily available with many electronic structure software packages. These hypotheses not only help us to understand the material's mechanic properties from a deeper and more fundamental level, but also serve as a basis to guide the selection of suitable nano-size metal oxides to be incorporated in the Mo or Cr alloys to achieve the desirable room-temperature ductility and to form the strategy for a systematic approach to enhance the material's properties for better performance.

In the following sections, we shall first present these hypotheses starting from the Rice's criterion, followed by our results of electronic structure analysis on Cr- and Mo-based alloy systems, where we will explain in detail about the impurity embrittlement and the observed ductility enhancement with the inclusion of MgO spinel, as demonstrated in Brady's experiments [3]. We conclude with discussions and a brief future work plan.

The Extensions Of Rice's Criterion

In transitional metal such as Cr and Mo, atoms are bonded by sharing their valence electrons. The Rice criterion suggests that if it costs less energy to assume a stacking fault configuration than to break the bonds, the material would be ductile. The stacking fault state creates layers of misaligned atoms, in which the chemical bonds between layers need to be stretched and distorted. To make this configuration energetically more favorable than the cleavage (bonds broken state), we anticipate that the electrons making up these bonds need to be delocalized and mobile so that they can easily follow the misaligned ions and refill the voids to preserve the bonds. To assess the mobility of the valence electrons near the Fermi level, we analyzed the following electronic properties:

(a) Electronic Charge Distribution (Real Space Distribution)

A more globally shared (delocalized) electron state is easier to reshape and adapt to the ionic displacement (like the stacking faults) than a localized state. In a Full potential linear muffin-tin orbital (FP-LMTO) calculation, the electronic charge is partitioned into muffin-tin (MT) spheres and interstitial areas. Charge in interstitial area is considered as being shared by ions, which contributes to ductile chemical bonds. Charge in the MT spheres may still be considered delocalized and beneficial to ductility if it is uniformly shared by many different MT spheres. To distinguish between localized and delocalized charge in the latter case, we calculate the variance of its population distribution among all MT spheres, and the smaller variance indicate better sharing. The results of this analysis are provided in Section 2.2.1. The extent of localization for a given electronic state may also be measured by entropy, defined as $S = - \sum n_i \log n_i$, where n_i is the partition of the charge on the i th atomic site. States with larger entropy are more mixed in space, and therefore more delocalized. This method is used in our larger scale molecular dynamic simulations in Section 2.2.4.

(b) Density of States (Energy Space Distribution)

The Density of States (DOS) provides another measure of mobility across the Fermi level. Due to

Pauli's exclusive principle, most of electrons are frozen in the low lying energy levels, while a small population of electrons immediately below the Fermi level may be excited into the empty orbitals (conduction bands) above the Fermi level. Electronic states in conduction bands are generally more delocalized and mobile. Therefore, the shape of DOS near the Fermi level can provide useful information for the characterization of chemical bonds and their mechanical properties. The results of this analysis are shown in Section 2.2.2.

(c) Angular Momentum Projected Population (Angular Momentum Space Distribution)

Chemical bonds formed by *s* electrons tend to be more flexible than those formed by *d* electrons. This is because the distribution of *s* electron has rotational symmetry, and the unstable stacking fault configuration may be assumed with the rotation and stretch of the bonds which costs little energy. In this case, the bonds are metallic and ductile. In contrast, chemical bonds formed by *d* electrons are strongly angular dependent. Any changes in the preferred bonding direction result in large energy penalty. Therefore the characteristics of the chemical bonds are more covalent-like, and brittle. By comparing the population of occupied angular channels, we may predict the ductile/brittle properties of the materials. The results of this analysis are shown in Section 2.2.3.

TASK I: RESULTS AND DISCUSSION

As shown in Figure 1, to study the mechanisms of the impurity and additives effects, we considered the following two model systems; (a) 1 x 1 x 3 Cr/Mo supercell containing one nitrogen/oxygen impurity at the center (Figure 1a), and (b) 1 x 1 x 3 Cr/Mo supercell interfaced with 6 stacks of MgO layers, with nitrogen/ oxygen impurities near the interface (Figure 1b)

Between these models, system (a) represents the impurity embrittled metal, while system (b) represents the ductility enhancement due to the inclusion of MgO. FP-LMTO techniques [6], which accurately treat the muffin-tin's interstitial region, have been used to calculate the electronic structures for the above systems. A three-kappa linked base is used to expand the muffin-tin tail functions. The energies for these bases are set to be -0.9, 0.3, and 1.2, respectively. Iterations are repeated until a convergence of 10^{-5} rydberg is achieved, after which the electronic charge density and DOS are obtained and analyzed.

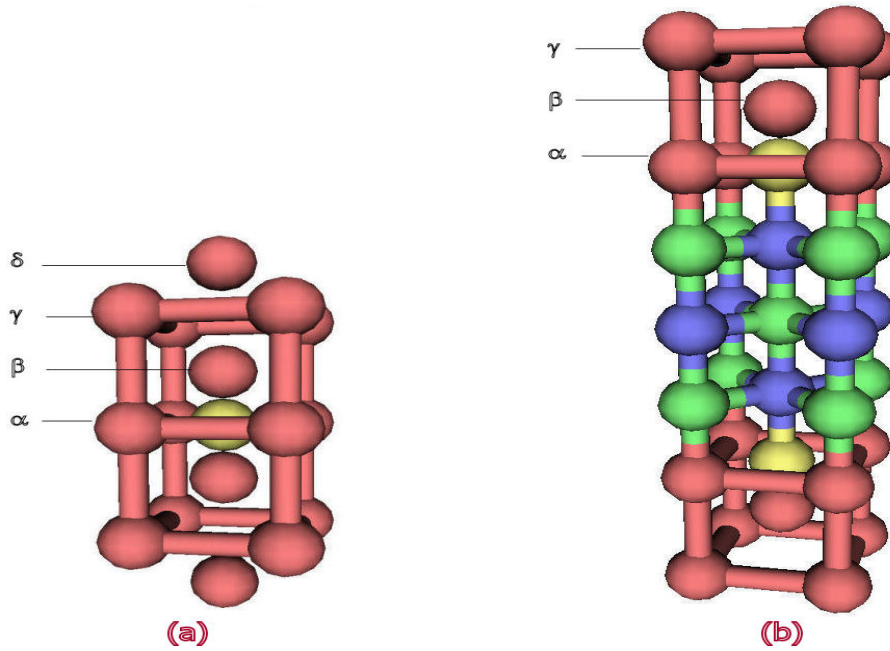


Figure 1. The schemes of the simulated systems: (a) a 1x1x3 Cr or Mo supercell (red spheres) containing a nitrogen or oxygen impurity (yellow sphere) at the center; (b) a 1x1x3 Cr or Mo supercell (top and bottom parts) interfaced with 6 stacks (figure only show 3 for simplicity) of MgO layers (center part, Mg and O atoms are represented by blue and green spheres, respectively), with two nitrogen or oxygen impurities (yellow spheres) near the interface.

Electronic Charge Distribution

The charge distribution of a given electronic state gives one some idea about how localized or delocalized an electron is. As discussed in Section 2.1, the distribution of a delocalized electron is easy to deform so as to preserve the chemical bonds should ions be misaligned. Therefore delocalized electrons contribute to the system's ductility. In FP-LMTO calculations, the charge distribution is conveniently partitioned into interstitial regions and muffin-tin spheres.

Table 1. The overall proportion of interstitial charge in Cr alloys.

	System (a)	System (b)
Proportion of interstitial charge	14%	16%

Table 2. The overall proportion of interstitial charge in Mo alloys.

	System (a)	System (b)
Proportion of interstitial charge	27%	35%

The Interstitial charge is shared by ions in system. Thus, they contribute the most to the ductile bonds. Tables 1 and 2 give the overall proportion of interstitial charge for electronic states within 0.1Ryd.

across the Fermi level. In both tables, the impurity embrittled system has lower proportion of charge in the interstitial than the ductility enhanced system.

The muffin-tin (MT) charge is distributed among the different MT spheres. Compared to the interstitial charge, it is more localized to ions. However, if a given electronic state has a uniform distribution among the MTs, it is still considered as being shared, and helps to “glue” the system together. Tables 3 and 4 show the average variance of MT charge distribution for electronic states within 0.1Ryd. across the Fermi level. In both tables, the system (b), with MgO layers, has lower variance, indicating the charge is shared more uniformly among the muffin-tins. This is in consistent with the system’s ductile behavior. Therefore, we conclude that the delocalized and uniformly distributed electrons tend to form ductile bonds that resist to cleavage.

Table 3. The average variance of MT charge distribution in Cr alloys.

	System (a)	System (b)
average σ^2	0.0139	0.0124

Table 4. The average variance of MT charge distribution in Mo alloys.

	System (a)	System (b)
average σ^2	0.0120	0.0039

Density Of States (DOS)

In Figure 2 and Figure 3 we present the results of DOS calculations for the Cr and Mo alloys systems, respectively. Both figures show enhanced DOS for Cr/Mo atoms near the impurity. A very distinctive feature is that the majority of DOS curves cross the Fermi line at their minima in system (a) while those crosses at maxima in system (b). Due to Pauli’s exclusion principle, the electrons will first occupy the levels below the Fermi line and leave those above Fermi line mostly unoccupied. The states corresponding to the unoccupied levels are less crowded and usually more mobile. As mentioned in Section 2.1, the mobile electrons are easy to deform and are beneficial to the ductility property. Thus, for systems with larger DOS at Fermi level (whose DOS crosses Fermi line at maxima), electrons will be easier to cross the Fermi line and assume such a mobile state, and consequently the system is ductile, and vice versa. This further explains the impurity embrittlement and ductility enhancement effects.

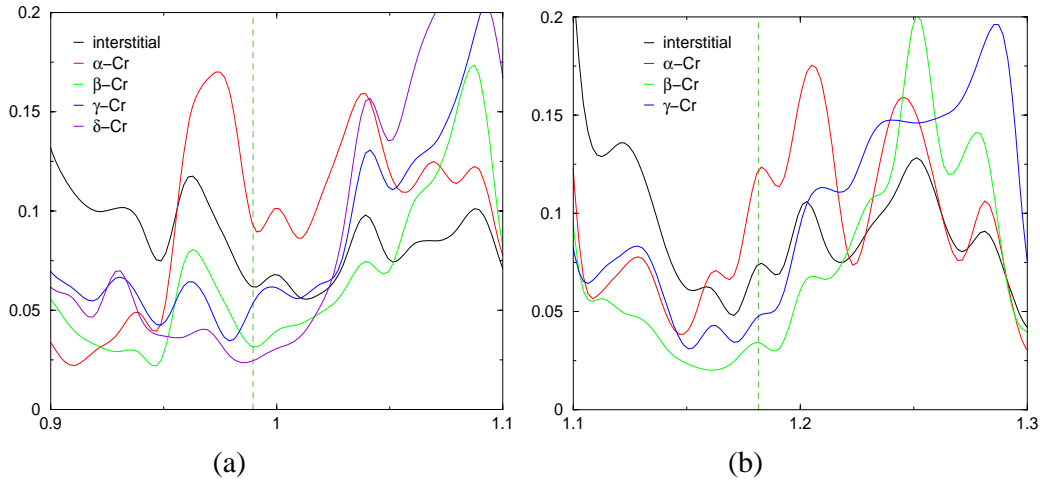


Figure 2: The DOS for Cr alloys.

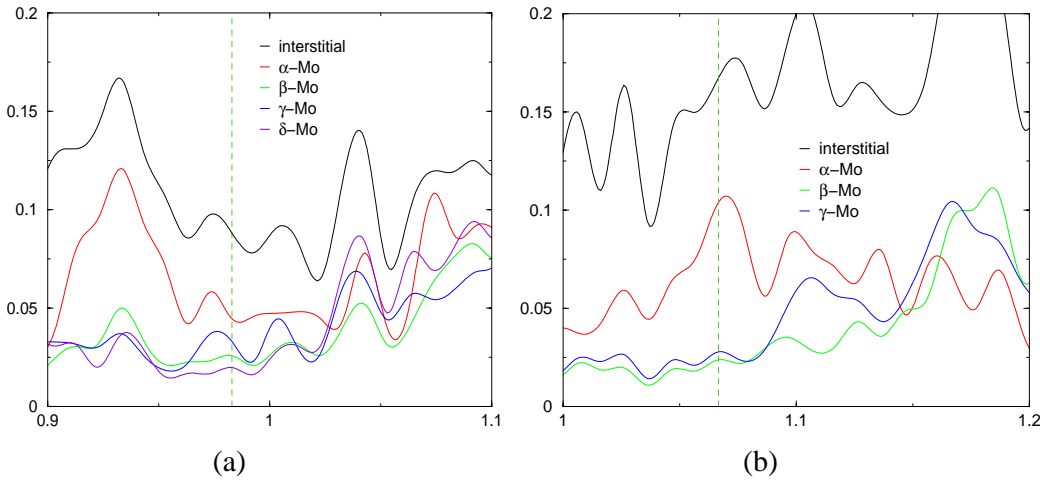


Figure 3. The DOS for Mo alloys

Angular Momentum Projected Population

The total charge population in both $4s$ and $3d$ angular momentum channels is determined for Cr in brittle and ductile systems, and the results are tabulated in Table 5. Comparing the columns, we find that both s and d channel charge population is increased due to the inclusion of MgO. Evidentially, the bond strength is enhanced. In addition, the increase of population in s channel is more prominent, and the s to d population ratio is also increased from 5.8% to 6.7%. Electrons in s angular momentum channel are isotropic in space. Correspondingly, bonds formed by s -electrons behave more like metallic bonds. On the other hand, bonds formed by d -electrons have strong directional preferences, which behave more like covalent bonds. The fact that metallic bonds render ductility and covalent bonds cause brittleness can be understood through Rice's criterion. In systems where metallic bonds dominant, the uniformly shared electrons are more tolerant with stacking faults; whereas in covalent materials, dislocation flow usually means breaking and reconnecting bonds with significant higher energy barrier. Assuming an equal energy cost to create

new surfaces by cleavage, the Rice ratio (γ_{us}/γ_0) is then higher in metallic systems than in covalent systems. Therefore, the ratio of *s* and *d* channel population is an indicative of whether the material shall display brittle or ductile behavior. By changing the balance of *s* and *d* channel charge population, MgO helps to improve Cr's mechanic properties.

Table 5. Calculated charge population in s and d channels (Cr alloy).

	System (a)	System (b)
<i>s</i> -channel	1.306	1.596
<i>d</i> -channel	22.503	23.738
Ratio <i>s/d</i> (%)	5.8%	6.7%

Molecular Dynamics Simulations

Using an *ab-initio* tight-binding electronic package called FIREBALL™ [7], we were able to extend the simulated system to a much larger scale, and carry out the molecular dynamics simulations to watch the system's evolution with time. FIREBALL™ is based on the density functional theory (DFT), and thus has the inherited accuracy comparable to other *ab-initio* methods. However, the computing time is significantly reduced because the Hamiltonian matrix elements have been expanded into one-, two-, and three-center integrals that are pre-computed into database for later interpolation. The many-body exchange-correlation potential and energy are treated similarly using a combined multi-center expansion [8] and linearization approximation approach. This scheme makes FIREBALL™ particularly efficient and capable of simulating larger scale systems such as nanostructures and DNAs.

Molecular dynamics simulations are carried out for Cr and Mo systems with the inclusion of MgO or spinel phase. In each of the systems, an impurity atom (N for Cr and O for Mo) is initially placed within the metal matrix. We then let the system freely evolve at constant temperature (set as 600°K), and watch the dynamics of the impurity atom. Figure 4 shows the initial and final configurations of Cr/MgO system after 1000 simulation steps (~1ps). The nitrogen impurity (marked as the orange sphere) was seen to gradually diffuse from the metal matrix to the metal/metal-oxide interfacial boundaries. This result is consistent with Brady's experiments, where they found the MgO tends to cause precipitations of N near the interface rather than actual getter of N as proposed by Schruggs who originally discovered the ductility enhancement effect [3]. Similar results have been found in the Cr/spinel system. In contrast, the Mo/MgO and Mo/spinel systems do not exhibit any oxygen diffusion. Therefore, alternative explanations of the observed ductility enhancement may be needed. Schneibel [9] has argued that grain size control among other issues is more important in affecting the mechanical properties for Mo-based systems. On the other hand, the inclusion of some other metal oxides is found to have impurity precipitation effects in Cr-based alloys however without any ductility improvement. This suggests the complexity of the problem, and necessary further investigations that are currently in progress.

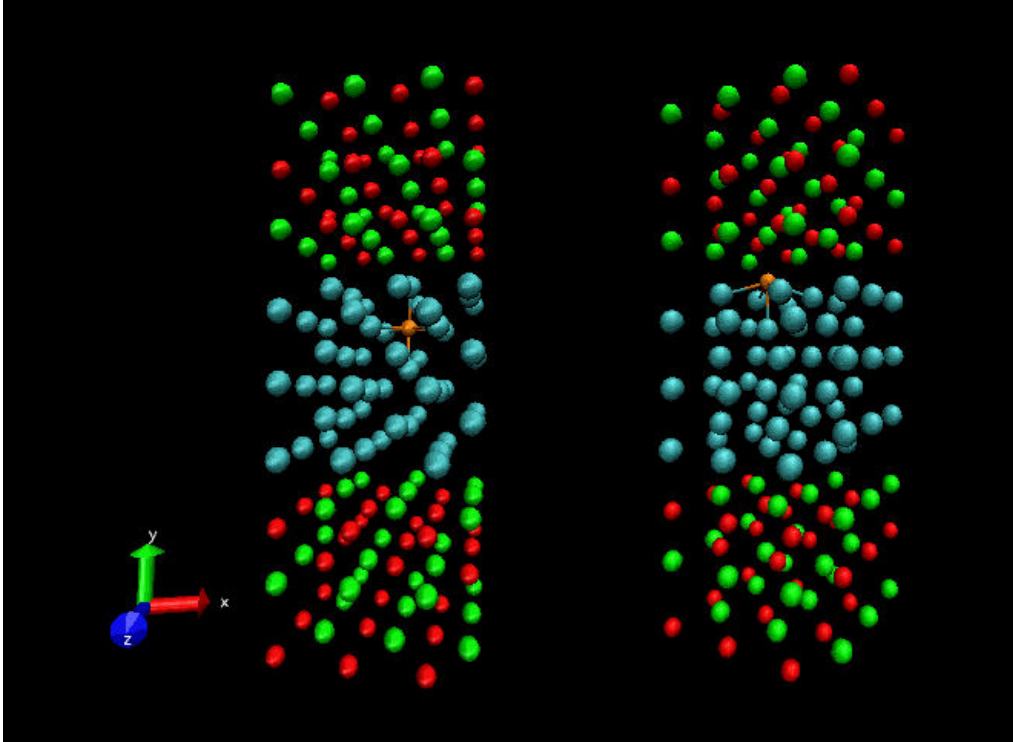


Figure 4: The diffusion of N in Cr/MgO system. Blue, green, red, and orange spheres represent, respectively, the Cr, Mg, O, and N species. The temperature is 600°K. Shown on the left is the initial system configuration, where the nitrogen impurity is placed inside the Cr matrix. The final system configuration after 1000 simulation steps (1ps) is shown on the right. The diffusion length is about 0.2 nm.

To understand how the position of impurity may affect the system's mechanic properties, we carried out the electronic structure analysis on both the initial and final configurations as shown in Figure 4. DOS and entropy have been computed for each electronic state near the Fermi level, and are presented in Figure 5. As explained in Section 2.1, DOS measures the mobility of the electrons while entropy depicts the overall spreading of charge in space. The total number of states within $\pm 1\text{eV}$ of the Fermi level is found to be 73 in the initial state and 76 in the final state. The average entropy for these states is 81.4 in the initial state and 83.9 in the final state, respectively. Evidentially, the diffusion of nitrogen atom indeed promotes both the mobility and uniform space distribution of the charge within the system. According to our criteria, the ductility should increase in the final state. This explains the ductility enhancement effects observed in Brady's experiments.

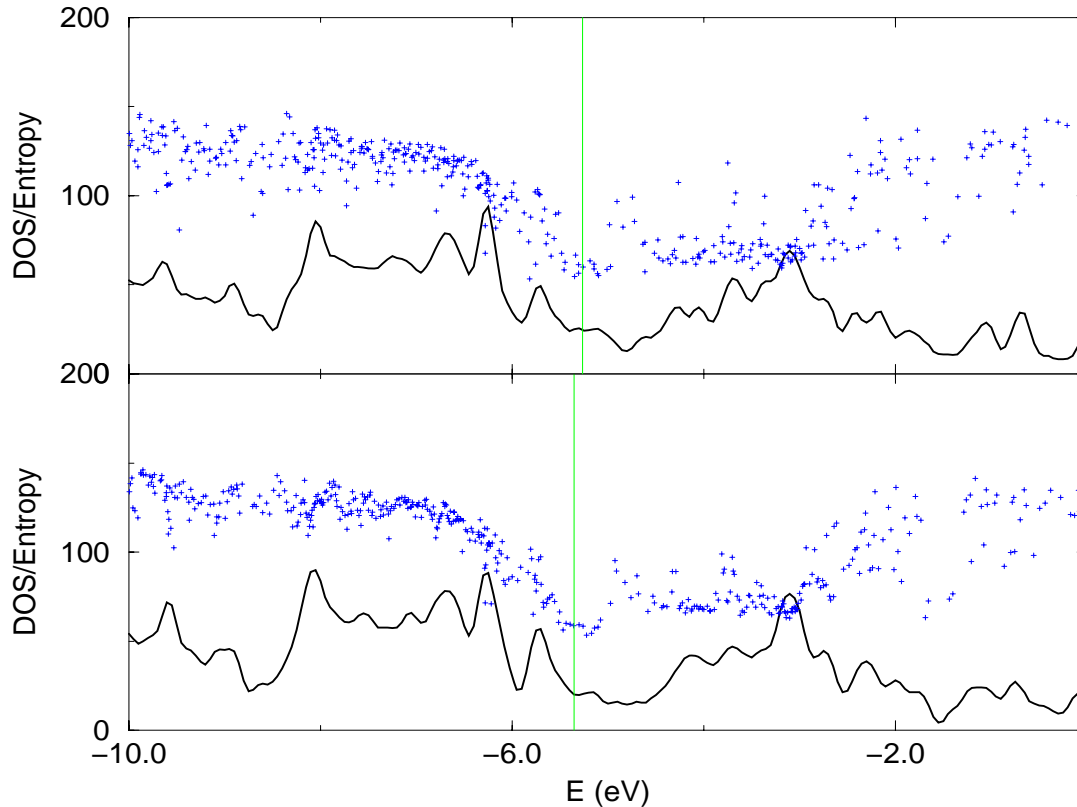


Figure 5. The computed density of state (black solid line) and entropy (blue pluses) plots for the initial (upper panel) and final (lower panel) configurations in Figure 4. The green vertical line represents the Fermi surface.

TASK I: CONCLUSIONS

Through atomistic modeling using FP-LMTO techniques, we obtained and compared the electronic structures of selected Cr/Mo systems containing N/O impurities and/or MgO layers. Several microscopic criteria have been identified to connect with material's ductile/brittle property. These include the extent of delocalization of the electronic state, the shape of the DOS curves near the Fermi level, and the angular momentum projected population. These criteria are shown to be in consistency with the Rice's criterion based on energetic arguments. Based on these criteria, we explained the impurity embrittlement and ductility enhancement effects due to N/O and MgO. These criteria are then used in larger scale (nano-scale) simulations to study other metal oxide dispersions as well as their size effects.

In-Situ Material Mechanical Property Measurement and Ductile/Brittle Characterization

In new alloys development using vacuum hot-pressed process such as the Mo and Cr alloys, many sample alloys are developed and needed to be tested for mechanical property evaluation. Current practice requires to prepare test specimen (with sufficient specimen size) in order to conduct tensile test to obtain the material Young's modulus and stress/strain curve. It would be advantageous to

develop a suitable material testing technique that is capable of obtaining mechanical properties and ductile/brittle evaluation on small-size (i.e. mm-size, such as 6 mm diameter and 6 mm long) sample alloys, this will greatly facilitate new alloys development. In this research task, a simple micro-indentation technique is developed to meet this goal.

Background

In material nano- and micro-indentation research, among all the indentation parameters, load-depth relation and unloading characteristics have been studied extensively either experimentally or numerically to elucidate the relevant mechanical behavior or properties. For example, it is well accepted to use the initial unloading stiffness of the load-depth curve to determine the material's Young's modulus [10-14]. This approach can be traced back to Sneddon's [10] classical elastic indentation solutions which describe the general relationship among the load, displacement and contact area for any punch that can be treated as a solid of revolution of a smooth function. In the 1970s, Bulychev and co-workers [11] defined the initial unloading slope and reduced modulus, thus providing a theoretically sound methodology for determining the Young's modulus. This method is applicable to both spherical and pyramidal indenters. Using instrumented indentations, Doerner and Nix [12] further investigated the unloading characteristics. In 1992, Oliver and Pharr [13] showed that Bulychev's technique can be applied to any indenter that can be described as a body of revolution of a smooth function.

In the indentation research for Young's modulus measurement, the contact area and initial unloading stiffness are the key parameters to be determined. However, in most cases, direct measurement of the contact area is not applicable or not possible. Typically, the unloading stiffness is used to estimate the contact area through some iterative algorithm [14-16]. Furthermore, high-precision displacement sensors are needed in order to accurately obtain load-depth curve and the unloading stiffness data [11-13]. As for the direct measurement of contact area, Kleesattel [17] designed a special apparatus for direct measurement of the contact region through a spherical sapphire indenter while conducting indentation tests, but the scanning method yields only one line of the contact region, and real-time access of the indented surface is not possible. By applying a special lighting technique, Frank [18] developed a transpyramidal indentation viewing system. It was also implemented by Sakaia et al [19] using a similar technique. Recently, with the support from the DOE/NETL Advanced Research Materials (ARM) Program, we have developed a Transparent Indenter Measurement (TIM) technique [20-23]. By integrating a Twyman-Green type interferometer into the spherical transparent indenter head, the TIM system can directly measure the indentation-induced out-of-plane deformation as well as the indented surface. It was found that by using the difference of out-of-plane deformation, Young's modulus can be evaluated without unloading stiffness measurement. Recently, a similar TIM approach was also done by Miyajima and Sakia [24] using sapphire spherical indenters on Aluminum and Zirconium oxide materials.

In this research, based on the experience learned from the research and development of the TIM technique, we have further developed a simple multiple partial unloading micro-indentation method for material's Young's modulus measurement. Experimental validation tests of several metallic alloys and related theoretical discussions are presented.

Multiple Partial Unloading Micro-Indentation Experimental Setup

Figure 6 shows the schematic of a simple indentation system. As shown, a spherical indenter assembly is attached to one end of the load cell, which is then attached to a PZT actuator. The PZT actuator serves as both loading apparatus and displacement sensing device. For the research work done in this paper, 1.5 mm diameter spherical indenters made of tungsten were used.

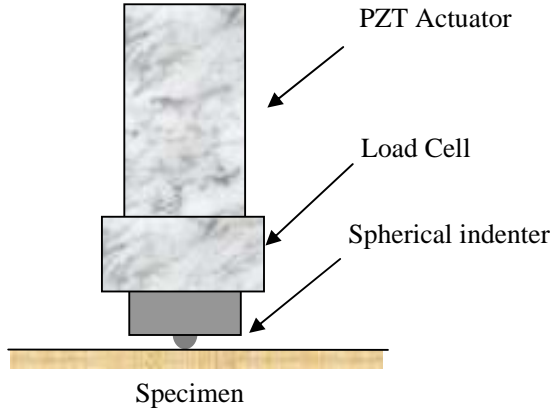


Figure 6. Load-displacement sensing indentation system.

A schematic load-displacement curve from the aforementioned experimental setup is shown in Figure 7. The PZT actuator provides the overall indentation depth (h) measurement, which includes both the indentation penetration depth and system deformation, i.e.,

$$h = h_i + h_s \quad (1)$$

where h_i is the indentation penetration depth and h_s is the loading system deformation.

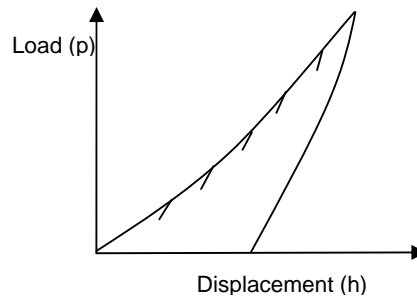


Figure 7. One indentation test with multiple partial unloadings.

At every unloading step (Figure 7), the unloading compliance is,

$$\frac{dh}{dp} = \frac{dh_i}{dp} + \frac{dh_s}{dp} = \frac{dh_i}{dp} + C_s \quad (2)$$

where C_s is the system compliance, which can be assumed to be a constant for a given system and within a given loading range.

Following the theoretical analysis of indentation [10-11, 14], the unloading compliance of a spherical indentation test can be expressed in terms of the indentation load, i.e.,

$$\frac{dh_i}{dp} = C \times \frac{1}{p^{1/3}} \quad (3)$$

where $C = (6RE_r^2)^{-1/3}$, R is the radius of the indenter, and E_r is the reduced modulus, defined by

$$\frac{1}{E_r} = \frac{1-\nu_i^2}{E_i} + \frac{1-\nu_0^2}{E_0}$$

E_i is the Young's modulus and ν_i is the Poisson's ratio of the test specimen, and subscript 0 denotes the indenter's mechanical properties. Substitute Equation (3) into Equation (2),

$$\frac{dh}{dp} = C \times \frac{1}{p^{1/3}} + C_s \quad (4)$$

Equation (4) shows that $\frac{dh}{dp}$ and $\frac{1}{p^{1/3}}$ has a linear relationship if C_s remains constant within a

given loading range, and thus measurement of slope C provides an alternative method for material Young's modulus measurement. It should be noted that, after obtaining the Young's modulus, other mechanical properties, such as hardness, stress-strain curve can also be determined [15].

For mechanical property measurement using instrumented nano/micro indentation technique, the effect of the system compliance is always a concern and this is why in-situ high precision and sometimes sophisticated displacement sensor is often used to remedy this problem. In this research, a rather simple approach is proposed to try to alleviate this problem by making the assumption that within a selected loading range (of an indentation test where data are collected for mechanical property evaluation) the system compliance is constant (i.e. load versus load-line system displacement is linear within the loading range). It should be noted that, experimentally, it is difficult to conduct direct measurement of the system compliance and thus prove the validity of this assumption. However, we noticed the investigation work of Oliver and Pharr [13] on system compliance measurement. Their approach is similar to what described in this paper, the difference is that instead of calculating the Young's modulus as proposed in this paper, it was used for system compliance determination.

In practice, Equation (4) also provides a convenient guideline to justify the validity of the proposed methodology, i.e., if the system compliance changes during the indentation loads, the linear relationship as depicted in Equation (4) can not be maintained.

EXPERIMENTAL INVESTIGATION

Test Procedure

Based on the aforementioned multiple partial unloading technique, a LabVIEW™ software tool is developed to conduct the indentation tests. The program will first detect the contact position between the indenter and the sample within a given load threshold (~0.1N), then it will conduct the multiple partial unloading indentation test using pre-defined parameters, such as the velocity of the indenter, the penetration depth and the unloading magnitude. After the completion of the indentation test, the program will process the data to determine the material Young's modulus from the slope measurement. For the results shown in this paper, all tests were conducted with six or ten loading/partial unloading steps, and each partial unloading displacement was either 0.5µm or 1µm, nominally.

Materials

To verify the feasibility of this technique, indentation tests were carried out on Al 7075-T6 and Inconel 783. The published Young's modulus values for Al 7075-T6 and Inconel 783 are 71.7GPa and 177.3 GPa, respectively [25, 26]. The Inconel 783 alloy had standard heat treatment (1120°C/1hr/AC + 845°C/8hrs/AC + 720°C/8hrs 50°C/hr 620°C/8hrs/AC). The Young's modulus of the sapphire indenter is 340GPa with Poisson's ratio equal to 0.29. Preliminary tests were then carried out on several research alloys, as listed in Table 6. As shown in Table 6, in addition to the ORNL alloys, three batches of Mo alloys were prepared at WVU using a sonication process. TiO₂ (~5 nm) and Mo (~65 nm) were taken as 5g and 95g respectively according to their weight percent ratio. Similarly 5g of MgO (~50 nm size) and 95g of Mo (~ 65 nm) were taken for the other composite. Then we followed the following procedure for assuring uniform mixing of the components. Mo was dissolved in ethyl alcohol and sonicated for 10 minutes in presence of Ar. Then TiO₂ was mixed slowly to the Mo solution with continuous sonication. The total mixture was sonicated for 1 hour in Ar atmosphere. The mixture was kept at room temperature for 1 day to remove ethanol. Finally it was dried in vacuum. In the same way we prepared the (MgAl₂O₄)_{0.05}(Mo)_{0.95} composite (~35 nm particle size of MgAl₂O₄). The dried powder samples were kept in Ar-filled glove box and packed in presence of Ar. These are the as-prepared sample powders which were sent to Dr. J.H. Schneibel at ORNL for vacuum hot-pressed casting.

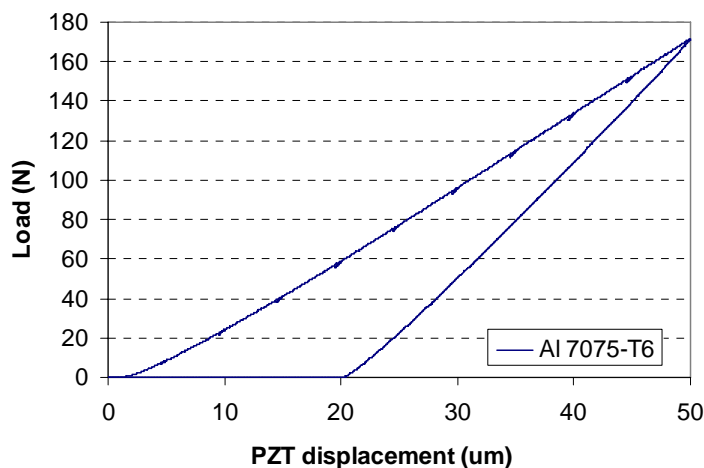
Table 6. Materials Matrix

(Alloys received from M.P. Brady and J. H. Schneibel, ORNL)	
#678, Mo-3.4wt%MgAl₂O₄	: 1800°C/4hr/3ksi/Vacuum, Mo powder 2-8µm, MgAl ₂ O ₄ , 1-5µm
#696, Mo-3.0wt%MgAl₂O₄	: 1800°C/1hr/3ksi/Vacuum, Mo powder 2-8µm, MgAl ₂ O ₄ , 1-5µm
#695, Mo only	: 1800°C/1hr/3ksi/Vacuum, Mo powder 2-8µm
#697, Mo-6.0wt%MgAl₂O₄	: 1800°C/1hr/3ksi/Vacuum, Mo powder 2-8µm, MgAl ₂ O ₄ , 1-5µm
#698, Mo-3wt%MgO	: 1800°C/1hr/3ksi/Vacuum, Mo powder 2-8µm, MgO, 1-5µm
Cast Re-(26-30) Cr wt% nominal:	1800°C/1hr/3ksi/Vacuum
(Powder mix prepared at WVU and sent to J.H. Schneibel for vacuum hot-pressed)	
WVU-1, Mo-5.0wt%MgAl₂O₄	: 1800°C/0.5hr/3ksi/Vacuum
WVU-2, Mo-5wt%MgO	: 1800°C/1.0hr/3ksi/Vacuum
WVU-3, Mo-5.0wt%TiO₂	: 1700°C/0.5hr/3ksi/Vacuum

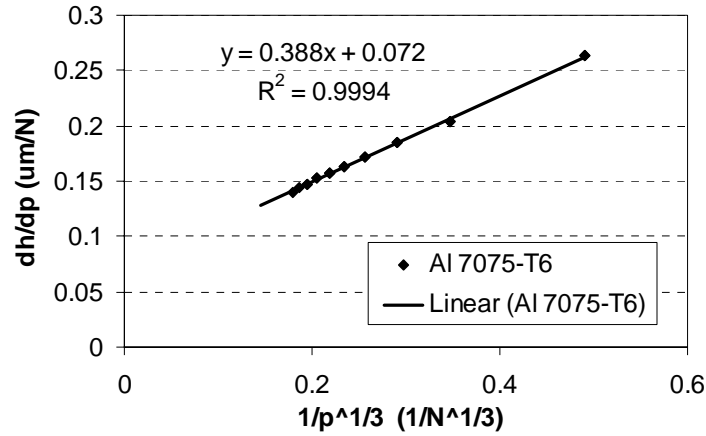
TASK II RESULTS

Al 7075-T6

Several indentation tests were carried out on the Al 7075-T6 alloy. Figure 8(a) shows the typical indentation load and displacement data, in which ten partial unloading/reloading were introduced. Based on the unloading line data, compliances at each unloading step were calculated. They were then further processed according to the algorithm discussed in the multiple partial unloading procedure. Figure 8(b) shows data analysis results based on Equation (4). The processed data show the existence of a linear relationship within most of the applied indentation loading range. Using the linear unloading line, Young's modulus was calculated by applying Equation (4) and assuming a Poisson ratio of 0.3. An average value of 67.2 GPa was obtained. The experimental data obtained are in good agreement with the book value of 71.7 GPa.



(a) Load-displacement curve with multiple-partial unloadings

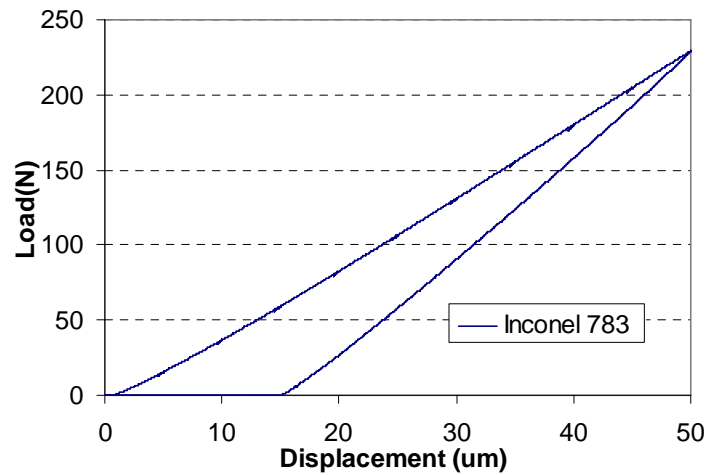


(b) Linear relationship

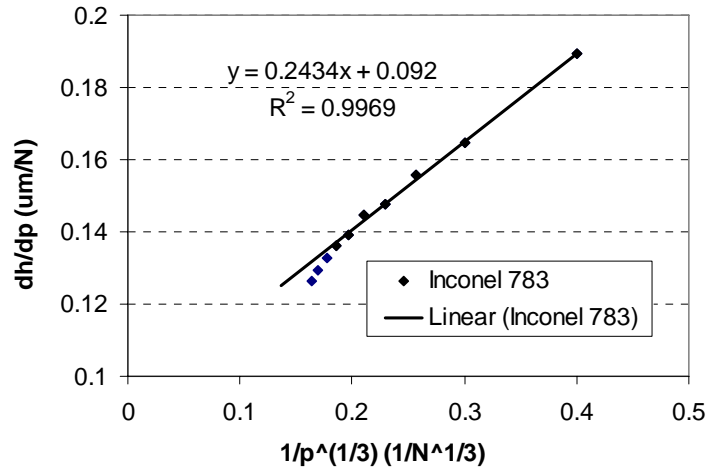
Figure 8. Experimental results for Al 7075-T6 alloy.

Inconel 783

Figure 9 shows the typical indentation test results for Inconel 783. In Figure 9(a), there were ten partial unloading displacements of 0.5 μm each. Based on the linear unloading line data, compliances at each unloading step were calculated and then further processed according to the multiple partial unloading technique. Similar to the Al 7075-T6 test, a linear relationship is observed within most of indentation loads, as show in Figure 9(b). However, the data starts to deviate from the linear relationship at higher indentation loads, indicating the breakdown of the constant system compliance assumption, as discussed earlier. Again, using only the linear part in Figure 9(b), and based on Equation (4), Young's modulus values were calculated. An average value of 168.4 GPa is obtained and agreed well with the book value of 177.3 GPa.



(a) Load-displacement curve with multiple-partial unloadings



(b) Linear relationship

Figure 9. Experimental results for Inconel 783 alloy.

Mo and Cr Alloys

Micro-indentation tests were carried out on several research alloys as listed in Table 6. The results were presented in Figure 10, Figure 11, and Table 7. As for ductile/brittle evaluation of these alloys, relatively larger indentation loads (400 N to 2000 N) were applied to the samples. The higher indentation load is to have a sufficient elastic rebounding (after indentation unloading) that may cause cracking at the region just outside the perimeter line of the indentation contact zone, if the material is brittle. Preliminary results show that for the ORNL alloys, alloy #678 is the only alloy with sufficient room-temperature ductility while other alloys are brittle as evidenced with indentation-induced cracking, as shown in Figure 12. The results are consistent with the research work of ref. 3 and ref. 9. As for the WVU alloys, preliminary results show that only WVU-3 has some degree of room-temperature ductility and the metal oxide dispersion is not uniform especially for WVU-1 and WVU-2, as shown in Figures 13 to 15. The non-uniform oxide dispersion may be due to the fact that the prepared powder mix was exposed in air for about 60 to 80 seconds when pouring the powder mix to the crucible for vacuum hot-pressed casting. Further research is planned to process the alloys without exposing the powder mix to air during the vacuum hot-pressed procedure.

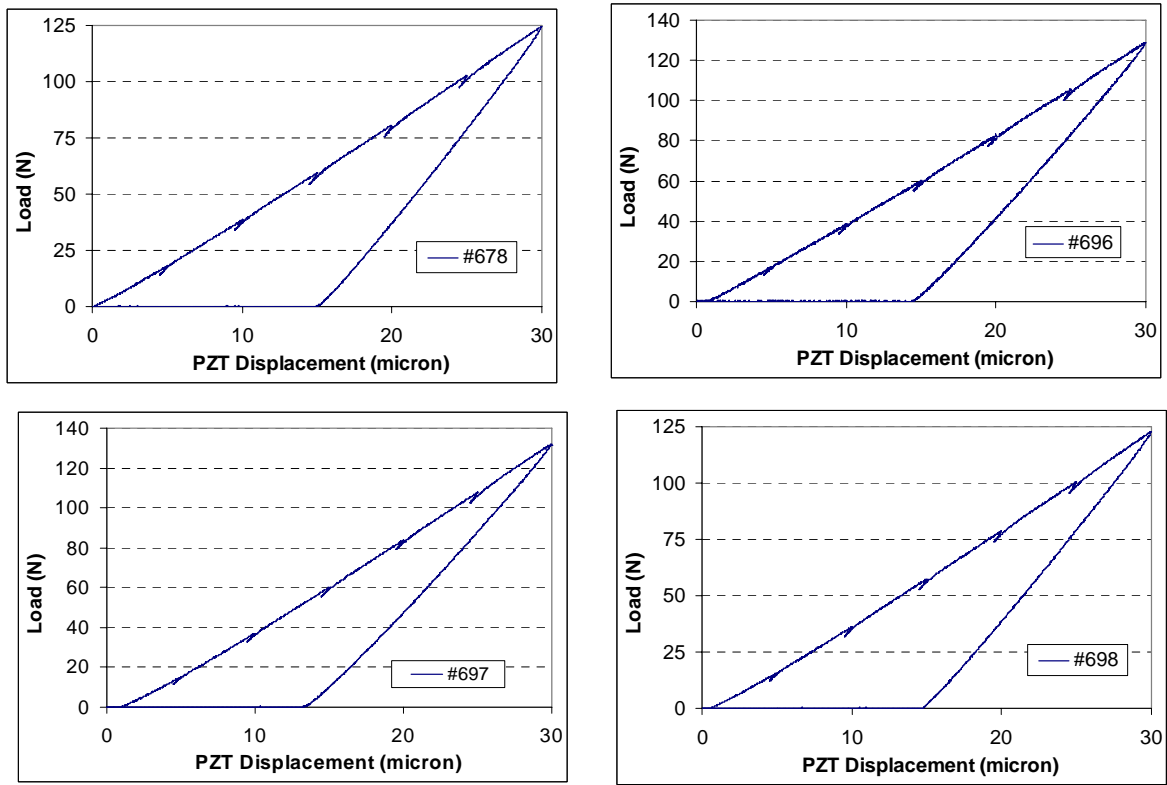


Figure 10. Typical load-displacement curve, ORNL Mo alloys, #678, #696, #697, #698.

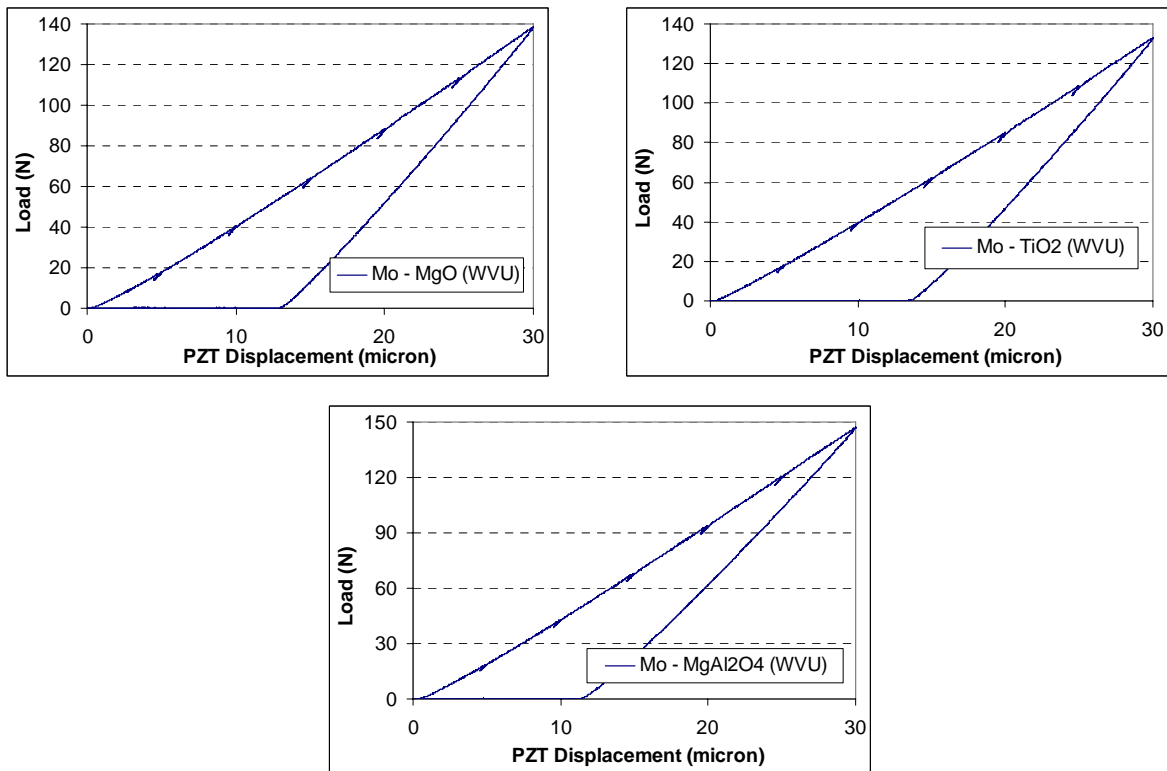


Figure 11. Typical load-displacement curve, WVU Mo-MgO, Mo-MgAl₂O₄, Mo-TiO₂ alloys.

Table 7. Summary - Young's Modulus Measurement

Material	Young's modulus (GPa)
Cast Re-(26-30) Cr wt%	234
#678, Mo-3.4wt% MgAl ₂ O ₄	229
#696, Mo-3.0wt% MgAl ₂ O ₄	200
#697, Mo-6.0wt% MgAl ₂ O ₄	192 (from tensile test : 189)
#698, Mo-3wt% MgO	211
WVU-1, Mo-MgO	254
WVU-2, Mo-TiO ₂	226
WVU-3, Mo-MgAl ₂ O ₄	202

(Averaged value from five indentation tests, typical)

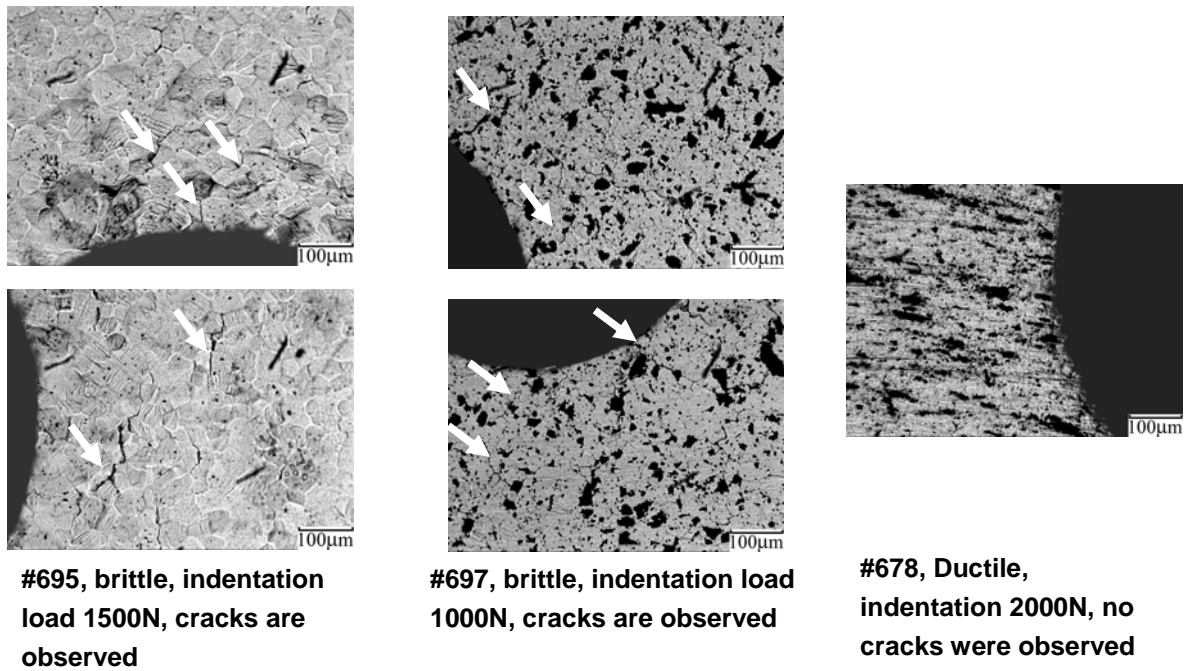


Figure 12. Material surface condition evaluation, ORNL Mo alloys.

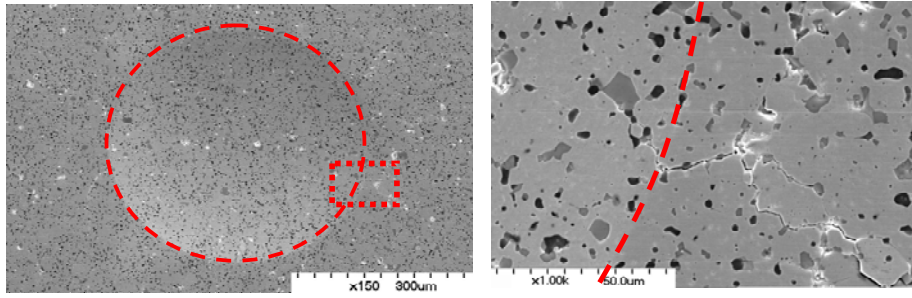


Figure 13 Ductile/brittle characterization using spherical micro-indentation Mo-MgO (WVU-1), 400N indentation, cracking.

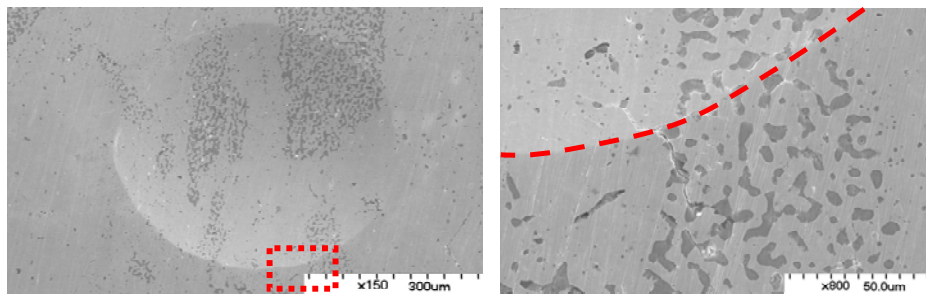


Figure 14 Ductile/brittle characterization using spherical micro-indentation Mo-TiO₂ (WVU-2), 400N indentation, cracking.

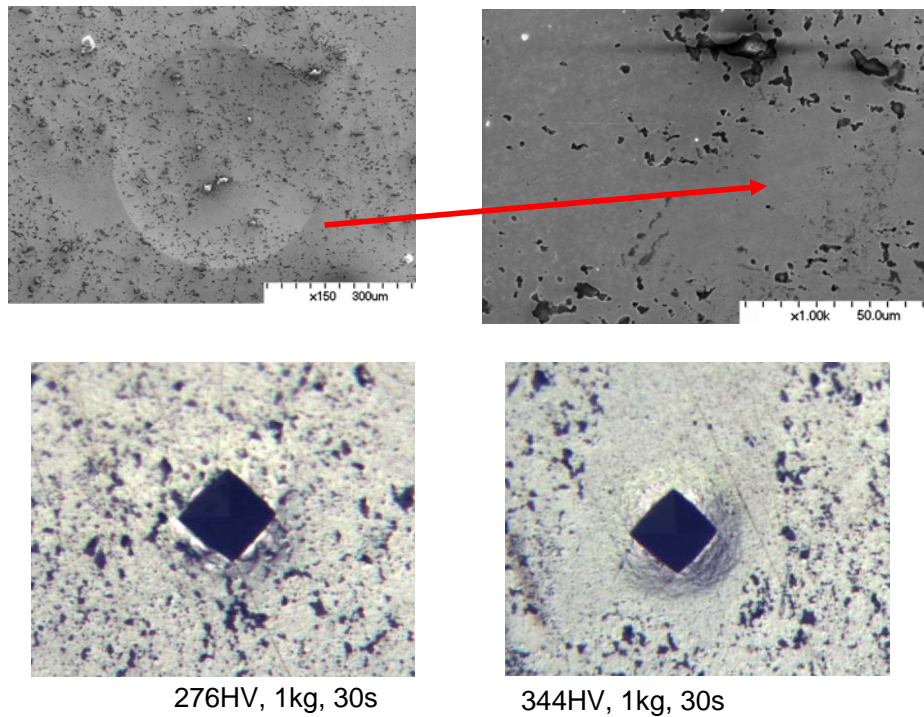


Figure 15 Ductile/brittle characterization using spherical micro-indentation
 Mo- $MgAl_2O_4$ (WVU-3), 400N indentation, no cracking.
 Vickers hardness tests show plastic flow at the matrix region.

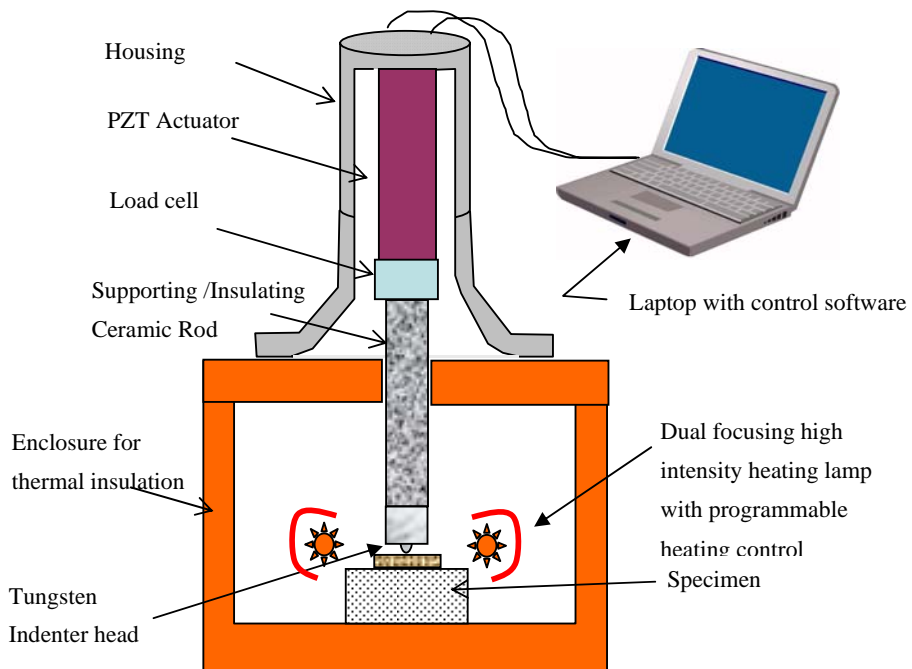


Figure 16. High temperature indentation using multi-partial unloading technique.

TASK II CONCLUSION

We present a simple multiple partial unloading micro-indentation testing method for in-situ surface material Young's modulus measurement and ductile/brittle evaluation on small-size alloys. Test results of two metallic alloys, (Al 7075-T6, and Inconel 783) show the validity of this technique. The proposed micro-indentation method does not require the use of sophisticated displacement sensor for indentation depth measurement and has the potential for the development of a portable micro-indentation instrument for on-site, in-situ component inspection and surface mechanical property evaluation. It can be configured for high temperature indentation test as schematically shown in Figure 16, which is under preparation with preliminary high temperature indentation tests planned for this project.

ACKNOWLEDGMENT

The work is sponsored by DOE Office of Fossil Energy, Advanced Research Materials (ARM) Program, under contract DE-AC05-00OR22725 managed by UT-Battelle, LLC. The research is also supported by DOE/NETL University Coal Research (UCR) Program under contract DE-FG26-05NT42526.

REFERENCE

1. W.D. Klopp, NASA TM X-1867, September (1969).
2. Y.F. Gu, H. Harada, Y. Ro, and T. Kobayashi, *Metal. & Mater. Trans. A* 36A, 577-582, (2005).
3. M.P. Brady, I.M. Anderson, M.L. Weaver, H.M. Meyer, L.R. Walker, M.K. Miller, D.J. Larson, I.G. Wright, V.K. Sikka, A. Rar, G.M. Pharr, J.R. Keiser, C.A. Walls, *Mater. Sci. & Eng. A* 358, 243-254, (2003)
4. A.A. Griffith, *Trans. First Intl. Cong. Appl. Mech. Delft*, 55-63, (1924)
5. J.R. Rice, *J. of the Mech. & Phys. of Sol. (UK)*, 40, 239-271, (1992)
6. D.L. Price and B.R. Cooper, *Phys. Rev. B* 39, 4945-4957, (1989); D.L. Price, J.M. Wills and B.R. Cooper, *ibid.* 46, 11368-11375, (1992).
7. J.P. Lewis, K.R. Glaesemann, G.A. Voth, J. Fritsch, A.A. Demkov, J. Ortega, and O.F. Sankey, *Phys. Rev. B* 64, 195103, (2001).
8. A. P. Horsfield, *Phys. Rev. B* 56, 6594-6602, (1997).
9. J.H. Schneibel, *Metal. & Mater. Trans. A* 34A, 25, (2003).
10. Ian N. Sneddon, "The relation between load and penetration in the axisymmetric Boussinesq problem for a punch of arbitrary profile," *Int. J. Engng Sci*, Vol. 3, pp. 47-57, (1965).
11. S.I. Bulychev, V. P. Alekhin, M. Kh. Shorshorov, A. P. Ternovskii and G. D. Shnyrev, "Determining Young's modulus from the indenter penetration diagram," *Industrial laboratory*, Vol.41, No.9, pp. 1409-1412, Sep. (1975).
12. M. F. Doerner, W. D. Nix, "A method for interpreting the data from depth-sensing indentation instruments," *J. Mater. Res.* 1(4), pp. 601-609, Jul/Aug, (1986).
13. W. C. Oliver; G. M. Pharr, An improved technique for determining hardness and elastic modulus using load and displacement sensing indentation experiments, *JOURNAL OF MATERIALS RESEARCH*, 7 (6), pp.1564-1583 June, (1992).
14. K. L. Johnson, *Contact Mechanics*, Cambridge University Press, (1985).

15. B. Taljat, T. Zacharia, "New analytical procedure to determine stress-strain curve from spherical indentation data," *Int. J. Solids structures*, Vol. 35, No. 33, pp. 4411-4426, (1998).
16. F. M. Haggag, "Field Indentation Microprobe for structural integrity evaluation," U.S. Patent No. 4,852,397, August 1, (1989).
17. Claus Kleesattel, "Method and apparatus for the measurement of hardness testing indentations," Patent No. 4,277,174, July 7, (1981).
18. Stefan Frank, "Transpyramidal indentation viewing - new possibilities for mobile hardness testing," 15th World Conference on Non-Destructive Testing, Rome, October, (2000).
19. M. Sakaia and N. Hakiri, T. Miyajima, "Instrumented indentation microscope: A powerful tool for the mechanical characterization in microscales," *J. Mater. Res.*, Vol. 21, No. 9, pp. 2298-2303, Sep., (2006).
20. C. Feng, B. S. Kang, "A transparent indenter measurement method for mechanical property evaluation," *Experimental Mechanics*, pp. 91-103, 46, (1), Feb., (2006).
21. C. Feng, B. Kang, "Young's modulus measurement using a simplified transparent indenter measurement technique," *Experimental Mechanics*, to be published.
22. B. S.-J. Kang, C.-Y. Feng, A. Manivannan, N. Ma, and B.R. Cooper, "In-situ mechanical property measurement and influence of impurity elements on grain boundary strength of Cr and Mo alloys," 19th Annual Conference on Fossil Energy Materials, May 9-11, (2005).
23. B. S.-J. Kang, N. Ma, C.-Y. Feng, and B.R. Copper, "In-situ mechanical property measurement and study of impurity embrittlement and metal oxides ductility enhancement mechanism in chromium alloys based on electronic structure analysis," 20th Annual Conf. on Fossil Energy Materials, June 12-14, (2006).
24. T. MIYAJIMA and M. Sakaia, "Optical indentation microscopy – a new family of instrumented indentation testing," *Philosophical Magazine*, Vol. 86, Nos. 33–35, pp. 5729-5737, Dec. (2006).
25. IN783 mechanical properties, <http://www.specialmetals.com>
26. Al 7075-T6 mechanical properties, <http://www.matweb.com>